ASTRONOMY & ASTROPHYSICS
SUPPLEMENT SERIES

Astron. Astrophys. Suppl. Ser. **117,** 303-312 (1996)

The dust distribution inside the Large Magellanic Cloud

M.O. Oestreicher and Th. Schmidt-Kaler

Astronomisches Institut, Ruhr-Universität Bochum, Universitätsstraße 150, D-44801 Bochum, Germany

Received August 15; accepted November 11, 1995

Abstract. — The distribution of the interstellar dust inside the LMC has been investigated on the basis of UBV photometry and spectral classifications of 1507 luminous O-A type stars. The mean internal reddening has been found to be rather high with $E_{B-V} = 0\overset{\mathrm{m}}{.}16$. The frequency distribution of the reddenings is strongly asymmetric, so that it is useless to give an error of the mean. Reddenings up to $0\overset{\mathrm{m}}{.}8$ have been observed. A strong selection effect is caused by the restricted visibility of strongly reddened stars. The intrinsically faint stars ($V_0 > 13\overset{\mathrm{m}}{.}3$) of our sample show no or low reddening $E_{B-V} < 0\overset{\mathrm{m}}{.}2$. Stars of intermediate brightness ($12\overset{\mathrm{m}}{.}3 < V_0 \leq 13\overset{\mathrm{m}}{.}3$) are reddened by up to more than $0\overset{\mathrm{m}}{.}3$. Reddenings between $0\overset{\mathrm{m}}{.}4$ and $0\overset{\mathrm{m}}{.}8$ occur for the intrinsically brightest stars ($V_0 \leq 12\overset{\mathrm{m}}{.}3$) only. According to the luminosity function the completeness limit of our sample has been found to be about $12\overset{\mathrm{m}}{.}$. To determine the reddening without bias, all intrinsically fainter stars have to be rejected. A comparison of the positions of highly reddened stars with $E_{B-V} > 0.3$ with those of molecular clouds detected by Cohen et al. (1988) shows few coincidences. Contrary to the dark cloud catalogues of Hodge (1972) and van den Bergh (1974) we detect highly reddened stars almost everywhere in the LMC. The frequency distribution of the reddenings can be fitted by a two cloud model. The mean reddenings caused by small and large dark clouds are $0\overset{\mathrm{m}}{.}04 \pm 0\overset{\mathrm{m}}{.}01$ and $0\overset{\mathrm{m}}{.}40 \pm 0\overset{\mathrm{m}}{.}10$, respectively. In the LMC, dust cloud properties are quite similar to those in the Galaxy. The number of small clouds on line of sight in comparison to that of large clouds is, however, higher than in the Milky Way. For the LMC we observe a number ratio of 45 ± 10 which may be compared with the galactic value of 9 ± 1. Finally we have determined a map of the internal reddening in the LMC. It shows overall agreement with that of Isserstedt & Kohl (1984), but gives higher absolute values, dominated by 30 Dor and the supershell LMC 2. Rather high reddenings have been found in the HII region N 11 and around the supershell LMC 6, too. Our map shows the same structure of the interstellar medium in the LMC as the HI map derived by Luks & Rohlfs (1992) and the IR emission maps derived by Israel & Schwering (1986).

Key words: galaxies: Magellanic Clouds — interstellar medium: extinction

1. The Data base

The UBV data and the spectral classifications were taken from the Bochum LMC Data Base (Gochermann et al. 1992). As almost all photometric observations were carried out using the Johnson system these data can be treated as rather homogeneous. The homogeneity of the observations carried out by the authors themselves is discussed in Oestreicher et al. (1995). The spectral classifications based on slit spectra can be treated as homogeneous (see Fitzpatrick 1988; Conti et al. 1986 and Massey et al. 1995). The classifications based on objective prism spectra, however, are rather inhomogeneous as already discussed by Ardeberg et al. (1972), Stock et al. (1976) and Rousseau et al. (1978).

2353 stars were available. After omitting all stars with uncertain photometry or spectral type or with spectral pecularities and all double and multiple systems, however, only 1507 stars remained.

Send offprint requests to: M.O. Oestreicher

To correct the photometric data for galactic foreground reddening the reddening map derived by Oestreicher et al. (1995) was used. Each star was treated individually. The intrinsic colour sequences and reddening lines of the luminous O to A type LMC stars were taken from Gochermann (1995).

2. Reddenings of single stars

The reddening of each star was derived both from spectral type and from the two-color-diagram (TCD). As the intrinsic colour sequences are luminosity dependent we compared the absolute magnitude M_v according to the given sequence with that according to the dereddened visual magnitude V_0 and the distance modulus of the LMC. If the difference $\triangle M_v$ of the two M_v changed its sign, we interpolated linearly between the two sequences. Otherwise we adopted the sequence with the smallest $\triangle M_v$.

To test the consistency of the data we plotted the reddening derived from the spectral type $E_{B-V,\mathrm{Sp}}$ over that

derived from the TCD $E_{B-V,\mathrm{TCD}}$ (Figs. 1 and 2). For O3 to B2 type stars (classified mainly by slit spectra) the agreement of the two data sets is very good. The scatter of the difference $\triangle E_{B-V} = E_{B-V,\mathrm{Sp}} - E_{B-V,\mathrm{TCD}}$ is only $0\overset{\mathrm{m}}{.}02$. For B3 to A6 type stars (classified mainly by objective prism spectra) we observe a larger scatter of $\triangle E_{B-V}$ with $0\overset{\mathrm{m}}{.}04$. For highly reddened stars with $E_{B-V} > 0\overset{\mathrm{m}}{.}3$ the reddenings derived from the spectral type are somewhat lower than those derived from the TCD. The extremely high values of about $0\overset{\mathrm{m}}{.}7$ to $0\overset{\mathrm{m}}{.}8$, however, are certainly real. The lower reddenings derived from the spectral type may be explained by the fact, that the classification of early type stars is often based not only on the occurrence of lines, but also on the appearance of the continuum. Thus a highly reddened star may be classified systematically too late. Since the UBV data are more homogeneous than the spectral classifications, the reddenings derived from the TCD were used for further analysis.

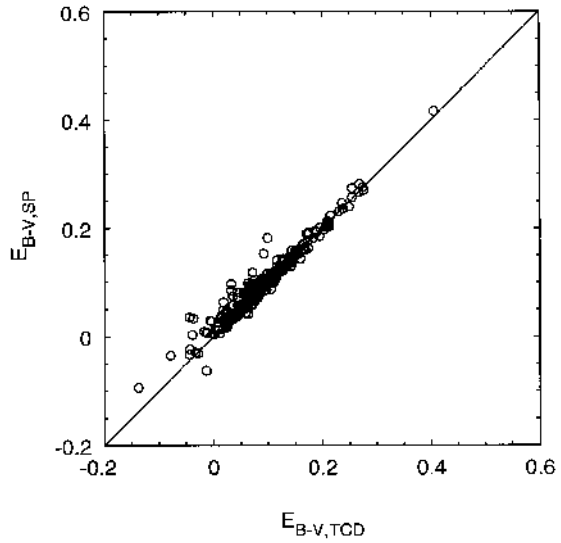

Fig. 1. Comparison of the reddenings derived from the spectral type with those derived from the TCD for O3 to B2 type stars. The solid line represents the relation $E_{B-V,\mathrm{Sp}} = E_{B-V,\mathrm{TCD}}$

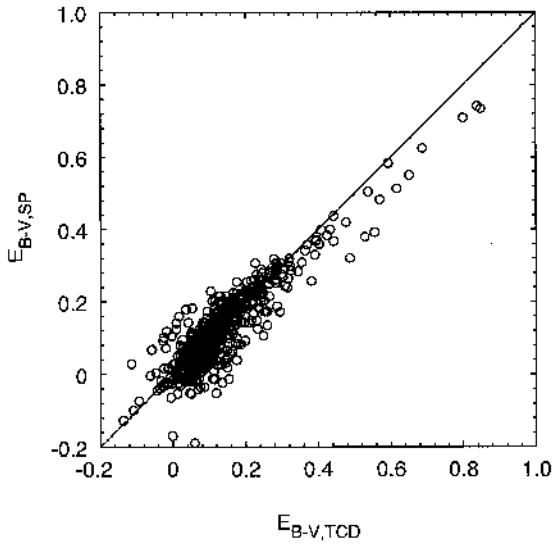

Fig. 2. Comparison of the reddenings derived from the spectral type with those derived from the TCD for B3 to A6 type stars. The solid line represents the relation $E_{B-V,\mathrm{Sp}} = E_{B-V,\mathrm{TCD}}$

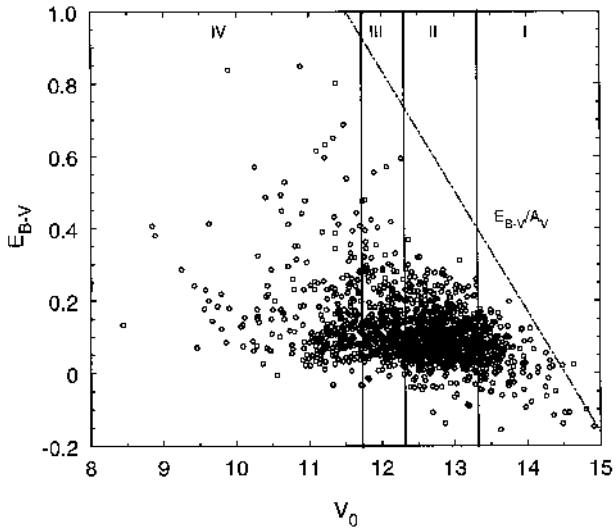

Fig. 3. Dependence of E_{B-V} on the absoption free magnitude V_0. The dashed line shows the visibility limit of our sample. The zones I to IV are explained in the text

To determine the amount of reddening in the LMC correctly, only stars intrinsically brighter than the completeness limit must be used. When going to intrinsically fainter stars, more and more highly reddened stars will escape detection. If all stars are included, the reddening will be underestimated. This effect is demonstrated in Fig. 3 where we plotted the reddening over V_0.

The increase of the mean reddening with increasing intrinsic brightness can be seen by dividing the stars into groups with different V_0. The intrinsically faint stars of group I ($V_0 > 13\overset{\mathrm{m}}{.}3$) show no or very low reddening. The frequency distribution of the reddenings does not differ much from an error population (Fig. 4). The mean reddening is $0\overset{\mathrm{m}}{.}05$. Stars of intermediate intrinsic brightness with $12\overset{\mathrm{m}}{.}3 < V_0 \leq 13\overset{\mathrm{m}}{.}3$ (group II) show already reddenings of up to more than $0\overset{\mathrm{m}}{.}3$. Their frequency distribution - which is presented in Fig. 5 - is significantly asymmetric. The mean reddening is found to be $0\overset{\mathrm{m}}{.}10$. For the intrinsically brightest stars with $V_0 \leq 12\overset{\mathrm{m}}{.}3$ (group III) reddenings higher than $0\overset{\mathrm{m}}{.}6$ are observed. The frequency distribution is extremely asymmetric (Fig. 6). The mean reddening is $0\overset{\mathrm{m}}{.}15$. If we restrict ourselves to stars with $V_0 \leq 11\overset{\mathrm{m}}{.}7$ (group IV) - where even reddenings higher than $0\overset{\mathrm{m}}{.}8$ occur - we find a mean reddening of $0\overset{\mathrm{m}}{.}17$ which is higher than all former investigations arrived at.

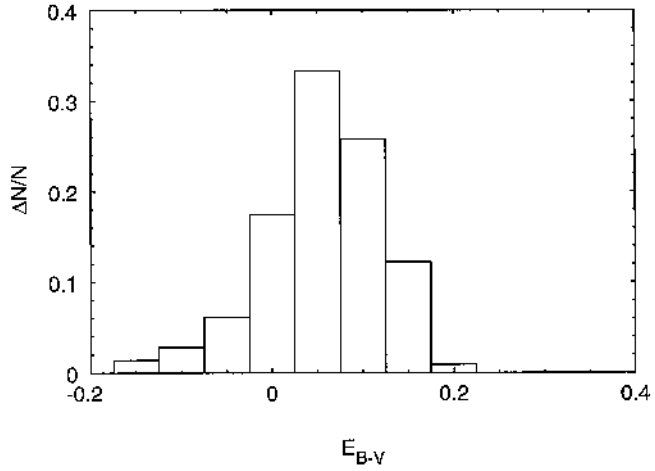

Fig. 4. The reddening distribution of intrinsically faint stars with $V_0 > 13\overset{\text{m}}{.}3$

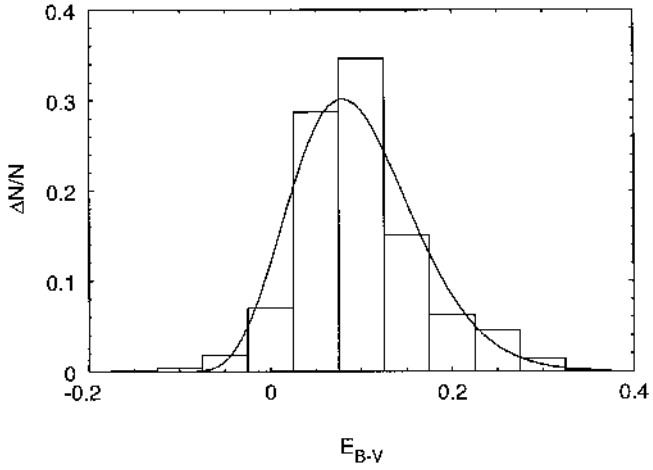

Fig. 5. The reddening distribution of stars of intermediate intrinsic brightness with $12\overset{\text{m}}{.}3 < V_0 \leq 13\overset{\text{m}}{.}3$. The solid line based on an one cloud model is explained in the text

One has to take into account, however, that very luminous stars may undergo heavy massloss and may therefore be additionally reddened by circumstellar dust shells. If we exclude the strongest reddenings $E_{B-V} > 0\overset{\text{m}}{.}4$ the mean reddening is still found to be $0\overset{\text{m}}{.}14$ and $0\overset{\text{m}}{.}15$ for group III and IV, respectively. An underestimation of the completeness limit leads also to an overestimation of the reddening. Therefore we also calculated the reddening with help of the luminosity function. Figure 7 represents the relative frequency $\triangle N/N$ and the cumulative relative frequency $\sum \triangle N/N$ in dependence on V_0. In Fig. 8 we show the plot $\log \sum \triangle N/N$ over V_0. The solid line breaks off for $V_0 > 12\overset{\text{m}}{.}0$ which agrees well with the completeness limit derived from the $E_{B-V} - V_0-$diagram.

The selection effect discussed here is one reason why up to now the reddening in the LMC was believed to be

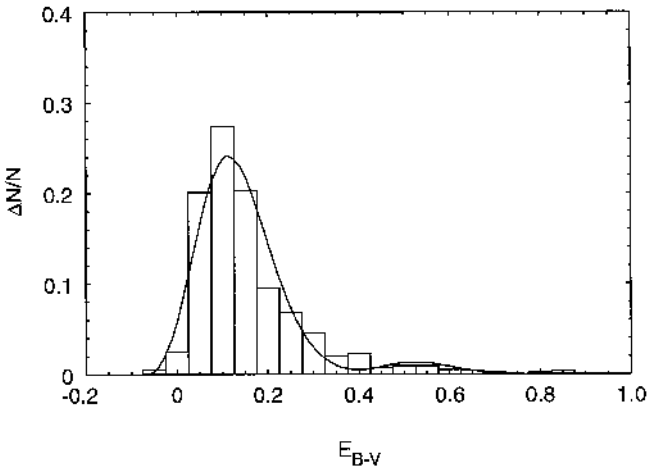

Fig. 6. The reddening distribution of intrinsically bright stars with $V_0 \leq 12\overset{\text{m}}{.}3$. The solid line based on a two cloud model is explained in the text

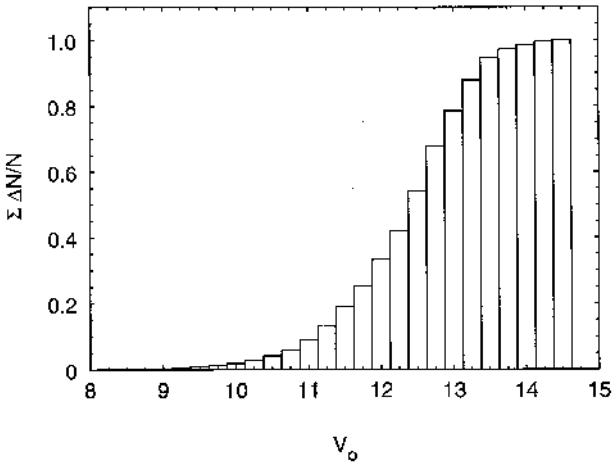

Fig. 7. The luminosity function of the luminous O3 to A6 stars in the LMC

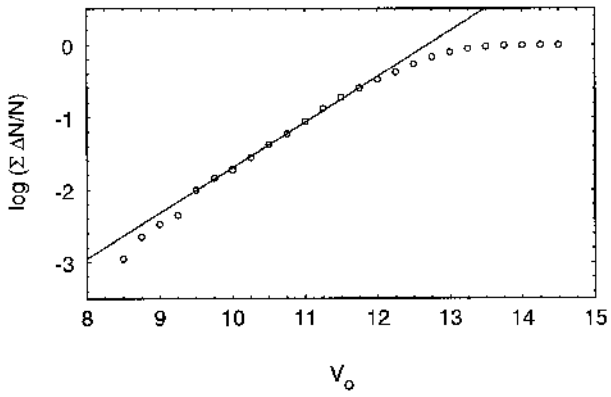

Fig. 8. The completeness limit of our sample. The linearity of the luminosity function breaks off at $V_0 = 12\overset{\text{m}}{.}$

rather low. Feast et al. (1960), Dachs (1972) and Grieve & Madore (1986) dealt with a much too small data sample to discuss it. Massey et al. (1995) treated a rather large data sample, but did not discuss the selection effect, too. Another error source is the use of galactic intrinsic colours. As the galactic supergiants are intrinsically redder than their counterparts in the LMC, this will lead to an underestimation of the reddening. Isserstedt 1975 treated the selection effect in a similar way as we, but adopted galactic intrinsic colours. Brunet (1975) and Isserstedt & Kohl (1984) used too red intrinsic colours again. The mean reddenings given by these authors are summarized in Table 1.

Table 1. Former investigations of the reddening inside the LMC. A "∗" indicates that the galactic foreground reddening was included. A "+" indicates that not the mean E_{B-V}, but the maximum of the E_{B-V} frequency distribution is given

Author	mean E_{B-V}
Feast et al. (1960)	$0\overset{m}{.}10*$
Dachs (1972)	$0\overset{m}{.}07*$
Isserstedt (1975)	$0\overset{m}{.}07* +$
Brunet et al. (1975)	$0\overset{m}{.}05$ ($0\overset{m}{.}03 - 0\overset{m}{.}11$)
Isserstedt & Kohl (1984)	—— ($0\overset{m}{.}02 - 0\overset{m}{.}20$)
Grieve & Madore (1986)	$0\overset{m}{.}10$
Massey et al. (1995)	$0\overset{m}{.}13*$
Our new value	$0\overset{m}{.}16$

Finally we plotted E_{B-V} over $(B-V)_0$ (Fig. 9). It can be seen that the highly reddened objects are mostly not O type stars but B and A type supergiants. Two possible but contrary explanations exist for that. On one hand the supergiants may be stars in the post red supergiant phase and may therefore be surrounded by circumstellar dust shells. In this case the mean reddening is slightly overestimated. On the other hand the supergiants are about $1\overset{m}{.}$to $2\overset{m}{.}$brighter than the O type stars. According to the selection effect thus highly reddened O type stars escape already detection when such supergiants are still visible.

To decide which explanation is more preferable we compared the positions of highly reddened stars with $E_{B-V} > 0\overset{m}{.}3$ with those of molecular clouds detected by Cohen et al. (1988) and of dark clouds detected by Hodge (1972) and van den Bergh (1974). Between the positions of highly reddened stars and molecular clouds only few coincidences were found as shown in Fig. 10. This may be explained as follows. Molecular clouds show often a very strong absorption of several magnitudes, so that stars situated deep inside them easily escape detection. Furthermore, the observations of Cohen et al. (1988) did not allow the detection of clouds with a diameter of less than 136 pc because of the resolution of $8'.8$. Of the 12 stars which are situated in or near molecular clouds, 3 (i.e. 25%) are O3 to B2 type stars while 9 (i.e. 75%) are B3 to A6 type

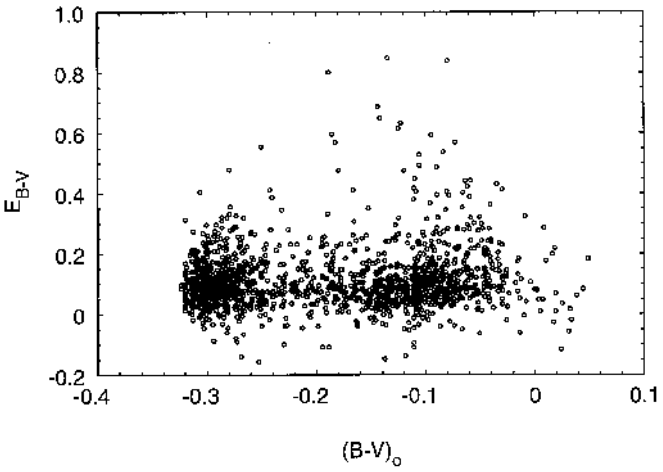

Fig. 9. The dependence of E_{B-V} on the intrinsic colour $(B-V)_0$

stars. The whole sample of highly reddened stars includes 51 objects of which 10 (i.e. 20%) are of type O3 to B2 and 41 (i.e. 80%) are of type B3 to A6. Therefore the youngest objects do not coincide more often with molecular clouds than the more evolved supergiants, suggesting that the extremely high reddenings of the latter are rather of interstellar than circumstellar origin.

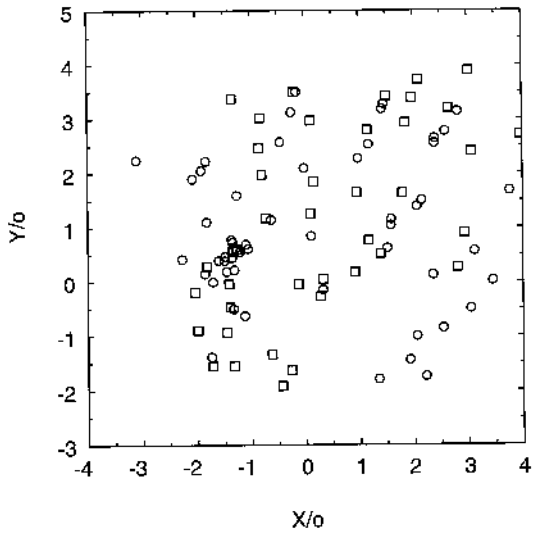

Fig. 10. The distribution of highly reddened stars and molecular clouds in the LMC. Stars are plotted as circles, molecular clouds as quadrangles. Cartesian coordinates according to Isserstedt (1975) are used

The comparison of the distribution of highly reddened stars with that of dark clouds detected by Hodge (1972) and van den Bergh (1974) is shown in Fig. 11. Contrary to these observations which show dark clouds in the inner

regions of the LMC only, we find highly reddened stars also in the outer regions. This may be explained by the fact, that the low surface brightness of the outer regions of the LMC prevents the detection of dark clouds on photographic plates, as discussed already by Hodge (1972) himself. In the inner regions, however, almost every highly reddened star coincides with a dark cloud. On the other side, only few dark clouds coincide with highly reddened stars, suggesting that many highly reddened stars escaped detection as already discussed above. 4 of the 14 stars which coincidence with a dark cloud are of type O3 to B2 (i.e. 28%) while 10 (i.e. 72%) are of type B3 to A6. The bluer stars do not coincide more often with dark clouds than the rest, confirming the interstellar origin of the high reddenings. To exclude a circumstellar origin definitively, however, additional IR observations are necessary.

Finally we compared the distribution of highly reddened stars with the spiral structure of the LMC described by Schmidt-Kaler (1977) (Fig. 12). Many of the highly reddened stars are situated in or near a spiral arm. Especially in the south east of the LMC, however, we find a group of several highly reddened stars for which no such counterpart exists.

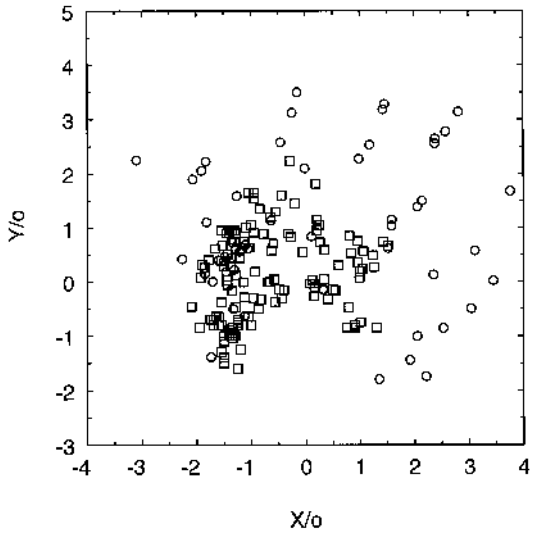

Fig. 11. The distribution of highly reddened stars and dark clouds in the LMC. Stars are plotted as circles, dark clouds detected by Hodge (1972) and by van den Bergh (1974) as quadrangles. Cartesian coordinates according to Isserstedt (1975) are used

3. The dark cloud structure in the LMC

The frequency distribution of the reddenings allows us to investigate dust cloud properties by applying the following model. Let us consider N types of clouds which cause reddenings $\epsilon_1, \epsilon_2, ..\epsilon_N$. For given numbers $n_1, n_2, ..n_N$ of clouds of type 1,2,..N on the line of sight the probability $\mathrm{p}(E)\mathrm{d}E$ to observe a reddening between E and $E+\mathrm{d}E$ is

$$\mathrm{p}(E)\mathrm{d}E = \delta(E - \triangle E) \tag{1}$$

with

$$\triangle E = \sum_{i=1}^{N} n_\mathrm{i}\epsilon_\mathrm{i} \tag{2}$$

The n_i follow Poisson distributions, i.e. we assume that the clouds are distributed at random and that the distributions of clouds of different types are independent from each other. Thus the probability q to observe fixed numbers $n_1, n_2, ..n_N$ of clouds is

$$q = \prod_{i=1}^{N} \frac{\lambda_{n_\mathrm{i}}^{n_\mathrm{i}}}{n_\mathrm{i}!}\mathrm{e}^{-\lambda_\mathrm{i}} \tag{3}$$

with λ_i the mean number of clouds of type i on the line of sight. The expected frequency distribution $f(E)$ then is given by

$$f(E) = \sum_{n_1,n_2,..n_N=0}^{\infty} \prod_{i=1}^{N} (\frac{\lambda_i^{n_i}}{n_i!}\mathrm{e}^{-\lambda_i})\, \delta(E - \triangle E) \tag{4}$$

$f(E)$, however, is not applicable because the reddenings have a mean observational error σ. $f(E)$ therefore has to be folded with a gaussian function. So we get the theoretical frequency distribution

$$F(E) = \frac{1}{\sqrt{2\pi}\sigma} \sum_{n_1,n_2,..n_\mathrm{N}=0}^{\infty} \prod_{i=1}^{N} (\frac{\lambda_\mathrm{i}^{n_\mathrm{i}}}{n_\mathrm{i}!}\mathrm{e}^{-\lambda_\mathrm{i}})\, \mathrm{e}^{-\frac{1}{2\sigma^2}(E-\triangle E)^2} \tag{5}$$

The unknown parameters $\sigma, \epsilon_1, \epsilon_2, ..\epsilon_n, \lambda_1, \lambda_2, ..\lambda_n$ can be calculated applying the statistical moments

$$\overline{E^\alpha} = \int_{-\infty}^{\infty} E^\alpha F(E)\mathrm{d}E \tag{6}$$

with $\alpha = 1,2,..2N+1$. The first three moments are given by the equations

$$\overline{E} = \sum_{i=1}^{N} \lambda_i\epsilon_i (\mathrm{mean}) \tag{7}$$

$$V = \sigma^2 + \sum_{i=1}^{N} \lambda_i\epsilon_i^2 (\mathrm{variance}) \tag{8}$$

$$S = V^{-\frac{3}{2}} \sum_{i=1}^{N} \lambda_i\epsilon_i^3 (\mathrm{skewness}) \tag{9}$$

Unfortunately the higher moments with $\alpha \geq 4$ are very sensitive to extremely high reddenings. Therefore the model can be applied without serious uncertainties for $N = 1$ only. Already for $N = 2$ five moments are needed.

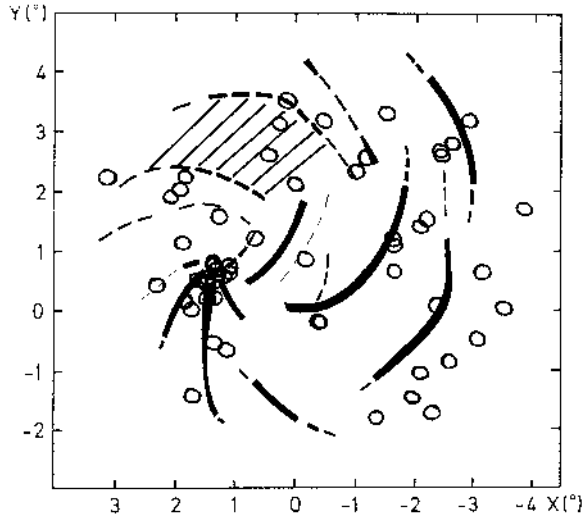

Fig. 12. The distribution of highly reddened stars and the spiral structure of the LMC. Spiral arms are schematically indicated according to their strength. Stars are plotted as circles. Cartesian coordinates according to Isserstedt (1975) are used

To avoid the large uncertainties introduced by higher moments we proceeded iteratively using just the selection effect discussed in the foregoing section.

The intrinsically faint stars of group I hardly allow the detection of dust clouds. The stars of intermediate brightness (group II) are assumed to be reddened mostly by small clouds causing a reddening ϵ_1. As no high reddenings occur among these stars, we can safely neglect the presence of large clouds which cause a reddening ϵ_2. Thus we have $N = 1$ and one can at once calculate σ, ϵ_1 and λ_1. ϵ_1 is an intrinsic property of the clouds and therefore independent from the selection of stars. Only λ_1 undergoes selection effects. The intrinsically bright stars of group III and IV are reddened by both small and large clouds. As σ and ϵ_1 can be taken from the distribution of the stars of group II, again three parameters only (ϵ_2, λ_1 and λ_2) are unknown.

Of course the definition of the groups I to IV is somewhat arbitrary. By shifting group II to lower luminosities, however, we get the same value for ϵ_1 in regard with the errors, only for λ_1 a little lower value is derived. By shifting group II a little to higher luminosities ϵ_1 remains unchanged again, but a higher λ_1 is calculated. If it is shifted, however, too far to the left in Fig. 3, no solution of the Eqs. (7-9) exists. Therefore the high reddenings can not be explained by the one cloud model confirming our assumption that at least two types of clouds are needed.

The statistical moments for all frequency distributions are given in Table 2. The cloud properties are presented in Table 3. The errors were calculated by drawing model curves with different parameter sets and comparing them with the observed distributions.

Table 2. Statistical moments of reddening distributions in dependence of the absorption free magnitude V_0. The groups I to IV are presented in Fig. 3

Group	V_0	mean E_{B-V}	variance	skewness
I	$> 13\overset{m}{.}3$	$0\overset{m}{.}051$	0.005	-0.283
II	$12\overset{m}{.}3 - 13\overset{m}{.}3$	$0\overset{m}{.}096$	0.004	0.541
III	$< 12\overset{m}{.}3$	$0\overset{m}{.}155$	0.016	2.179
IV	$< 11\overset{m}{.}7$	$0\overset{m}{.}171$	0.021	2.079

Table 3. Dust cloud properties in the LMC

Cloud type	reddening ϵ	number on line of sight λ
Small clouds	$0\overset{m}{.}04 \pm 0\overset{m}{.}01$	3.3 ± 0.5
Large clouds	$0\overset{m}{.}40 \pm 0\overset{m}{.}10$	0.06 - 0.10

From the stars of group II we calculate $\sigma = 0\overset{m}{.}022 \pm 0\overset{m}{.}005, \epsilon_1 = 0\overset{m}{.}040 \pm 0\overset{m}{.}010$ and $\lambda_1 = 2.4 \pm 0.5$. The observed distribution is fitted very well. The distributions of the stars of group III and IV give $\epsilon_2 = 0\overset{m}{.}40 \pm 0\overset{m}{.}10$ and $\epsilon_2 = 0\overset{m}{.}41 \pm 0\overset{m}{.}10$, respectively. λ_1 is found to be 3.3 ± 0.5 in both cases. The uncertainty of the completeness limit does not enter into these two parameters. This is not so for λ_2. We derive values of 0.059 ± 0.020 and 0.096 ± 0.020 for group III and IV, respectively. The mean ratio λ_1/λ_2 is found to be 45 ± 10. Additionally one has to take into account that the nature of the high reddenings is still not fully clear. If it would be mainly circumstellar, λ_2 is overestimated, i.e. very few large clouds would exist in the LMC. If it is interstellar, λ_2 is underestimated because of the partial lack of highly reddened O type stars.

A further source of underestimation of λ_2 may be the fact that we have excluded double and multiple systems which are often situated in star formation regions embedded in large clouds. To test this we tried to deal with these stars as single objects. As members of associations have almost the same age, we may assume that they have similar intrinsic colours as long we restrict ourselves to systems which do not contain red supergiants. Examples are the multiple systems HDE 269676 and HD 32228 which were observed by Heydari-Malayeri & Hutsemekers (1991) and Parker et al. (1992), respectively. Another systematic error is introduced by assuming the integral magnitude. As the intrinsic colours become redder with increasing luminosity the overestimation of the luminosity leads to an underestimation of the reddening. An error of $1\overset{m}{.}$in M_v leads to an error of about $0\overset{m}{.}03$ in E_{B-V}. The consistency of the reddenings derived from spectral type with those derived from the TCD is as good as for the single stars (Fig. 13 and Fig. 14). For O3 to B2 type stars the scatter

of $\triangle E_{B-V}$ is $0\overset{\mathrm{m}}{.}01$ only while for B3 to A6 type stars it is $0\overset{\mathrm{m}}{.}03$. Therefore we may assume that the systematic errors are small enough to allow statements about the frequency of large reddenings. Like in the case of single objects for stars with $E_{B-V} > 0\overset{\mathrm{m}}{.}3$ the reddenings derived from the spectral type are somewhat lower than those derived from the TCD. The frequency distribution of the reddenings of the double and multiple stars brighter than the completeness limit - which was determined to be the same as for the single stars - is presented in Fig. 15. A comparison with Fig. 6 shows that the fraction of highly reddened objects with $E_{B-V} > 0\overset{\mathrm{m}}{.}4$ is 10%, somewhat higher than for single objects. For the latter only 5.6% of the stars have reddenings higher than $0\overset{\mathrm{m}}{.}4$. The reddening distribution for the double and multiple objects can be fitted with $\sigma = 0\overset{\mathrm{m}}{.}04$, $\epsilon_1 = 0\overset{\mathrm{m}}{.}04$, $\epsilon_2 = 0\overset{\mathrm{m}}{.}30$, $\lambda_1 = 3.0$ and $\lambda_2 = 0.20$. For these we determine $\lambda_1/\lambda_2 \approx 15$ which is closer to the galactic value. As the number of double and multiple objects in our sample is only about $\frac{1}{4}$ of that of the single ones, however, this fact does not give a large contribution to the frequency of large clouds in general.

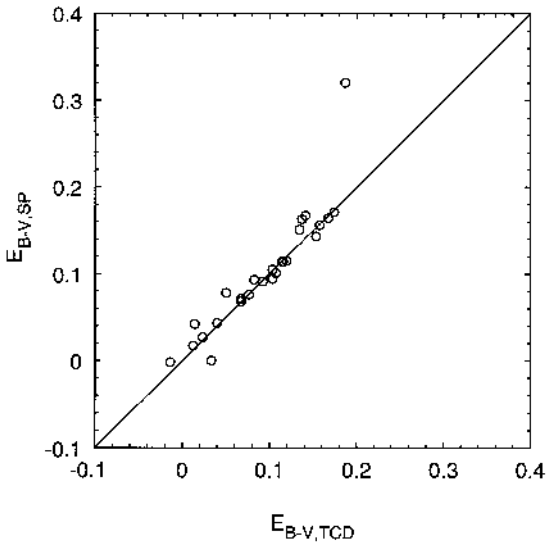

Fig. 13. Comparison of the reddenings derived from the spectral type with those derived from the TCD of O3 to B2 type double or multiple stars. The solid line represents the relation $E_{B-V,\mathrm{Sp}} = E_{B-V,\mathrm{TCD}}$

The observed distribution of the intrinsically bright stars is modelled well for $E_{B-V} < 0.3$ only. One has to keep in mind that the number of stars with higher reddenings in our sample (51 objects) is small, so that large statistical fluctuations may vitiate our results as concerns the large clouds.

Finally we compared our results with investigations of galactic dust cloud structure summarized in Table 4 and Table 5. The mean reddening caused by small galactic dust clouds is $0\overset{\mathrm{m}}{.}07 \pm 0\overset{\mathrm{m}}{.}02$, that caused by large clouds

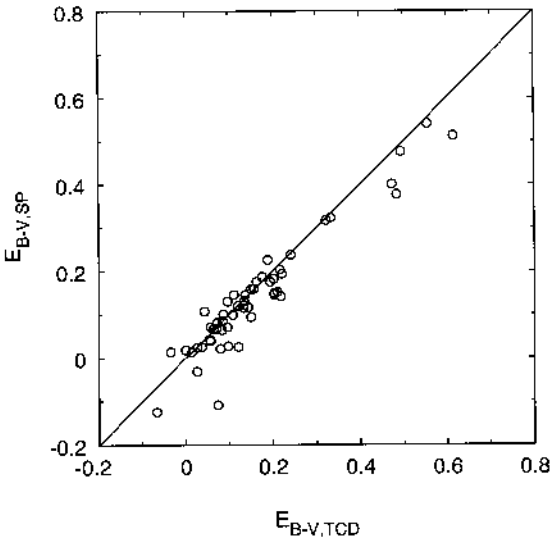

Fig. 14. Comparison of the reddenings derived from the spectral type with those derived from the TCD of B3 to A6 type double or multiple stars. The solid line represents the relation $E_{B-V,\mathrm{Sp}} = E_{B-V,\mathrm{TCD}}$

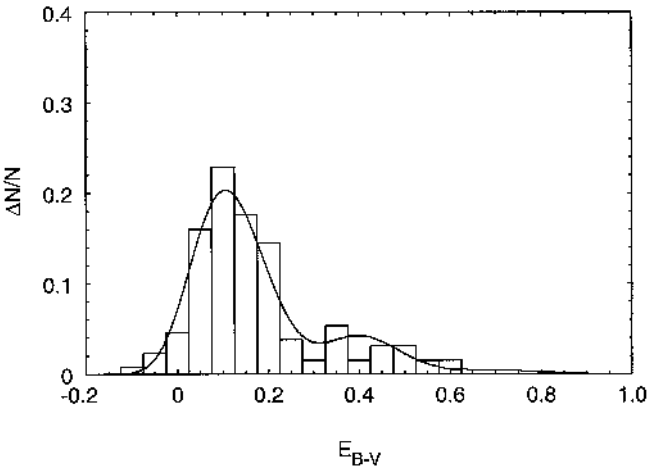

Fig. 15. The reddening distribution of intrinsically bright double or multiple stars with $V_0 \leq 12\overset{\mathrm{m}}{.}3$

$0\overset{\mathrm{m}}{.}44 \pm 0\overset{\mathrm{m}}{.}15$. These results agree with our investigation. So in the LMC dust clouds have similar properties as in the Galaxy. The ratio λ_1/λ_2, however, is found to be higher than in the Milky Way. We find $\lambda_1/\lambda_2 = 45 \pm 10$ while the galactic value is 9 ± 1. For double and multiple objects λ_1/λ_2 agrees with the galactic value. In general, however, large clouds are less frequent in the LMC than in the Milky Way, as the fraction of the double and multiple objects is only about $\frac{1}{5}$ of the whole sample.

We tried to deal with a continuous spectrum of clouds with mean number $\lambda = \lambda(\epsilon)$ in the line of sight. In this case one has to substitute the sums in the momentum

Table 4. Investigations of small dust clouds in the Galaxy

Author	ϵ_{B-V}	λ/ kpc
Schatzman (1950)	0.09	6
Münch (1952)	0.06 - 0.07	6.0 - 6.5
Scheffler (1967a)	0.08	5
Hobbs (1974)	0.11	4.6
Spitzer (1978)	0.06	6.2
Knude (1979a,1979b)	0.04	6 - 8
Mean values	0.07 ± 0.02	5.8 ± 0.8

Table 5. Investigations of large dust clouds in the Galaxy

Author	ϵ_{B-V}	λ/ kpc
Schatzman (1950)	0.66	0.6
Münch (1952)	0.25 - 0.38	0.6 - 1.0
Scheffler (1967a)	0.50	0.5
Spitzer (1978)	0.29	0.8
Mean values	0.44 ± 0.15	0.7 ± 0.1

equations by integrals. The simplest continuous model is that of an exponential law

$$\lambda(\epsilon) = \frac{1}{\beta} \mathrm{e}^{-\frac{\epsilon}{\beta}} \tag{10}$$

with β the mean reddening caused by a dust cloud. It works with only three parameters, σ, β and the mean total number

$$\lambda_{\mathrm{tot}} = \int_0^\infty \lambda(\epsilon) \mathrm{d}\epsilon \tag{11}$$

of clouds in the line of sight. This model, however, cannot be applied to the distributions of group III and IV, as Eq. (8) will lead to an imaginary σ because of the very large skewness. The spectrum $\lambda(\epsilon)$ decreases slowlier than according to an exponential law. This agrees with investigations of galactic dust cloud properties, which describe the spectrum as a combination of power laws (see e.g. Scheffler 1967b). We tried to fit our data with a power law but failed because of our small sample of highly reddened stars.

4. The LMC reddening map

Not only dust cloud properties, but also the distribution of the dust itself is important for understanding the structure and dynamics of the LMC. To investigate it, one should only use stars brighter than the completeness limit as discussed in Sect. 2. Therefore only 558 stars were available to determine the reddening map.

A first overview of the dust distribution is obtained by plotting stars of different reddenings (Fig. 16). The concentration of highly reddened stars to the 30 Dor region (position (−1.3, 0.3) in Fig. 16) and the supershell LMC 2 (−1.6, 0.3) is conspicuous. Nevertheless such stars exist almost everywhere in the LMC. Stars with low reddening, however, are almost absent in the 30 Dor region. The supershell LMC 4 (−0.7, 2.9) behaves inversely. Most stars observed there have low reddenings, stars with high reddenings are almost absent. In the bar both, low and highly reddened stars can be seen.

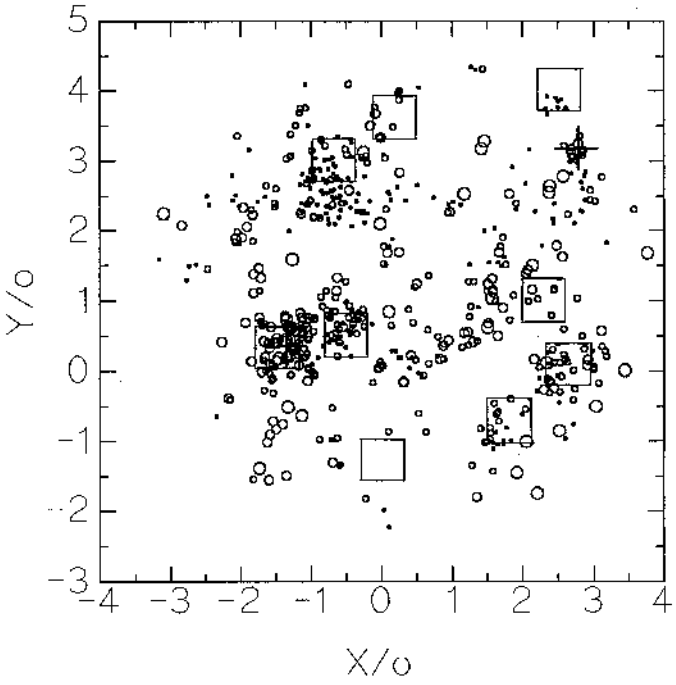

Fig. 16. The distribution of the stars brighter than the completeness limit at the sky. The largest circles represent stars with reddenings higher than $0\overset{\mathrm{m}}{.}4$, the following circles such with $0\overset{\mathrm{m}}{.}4 > E_{B-V} \geq 0\overset{\mathrm{m}}{.}2$, $0\overset{\mathrm{m}}{.}2 > E_{B-V} \geq 0\overset{\mathrm{m}}{.}1$ and $E_{B-V} \leq 0\overset{\mathrm{m}}{.}1$, respectively. The 30 Dor region and the HII region N 11 are marked with crosses, supershells with large quadrangles. Cartesian coordinates according to Isserstedt (1975) are used

To calculate a reddening map $E_{B-V}(\alpha, \beta)$ we determined the mean reddening of a fixed number N of stars situated closest to (α, β). The map for $N = 20$ is presented in Fig. 17. For smaller N the map shows more details, but due to the errors these may not all be real.

The highest reddening occurs in the regions of 30 Dor and the supershell LMC 2, where $E_{B-V}(\alpha, \beta)$ reaches a maximum of $0\overset{\mathrm{m}}{.}29$. The lowest reddening is observed in the region of the supershell LMC 4 with $E_{B-V}(\alpha, \beta) = 0\overset{\mathrm{m}}{.}06$. Further structures can be identified on the map. The HII region N 11 shows also a high reddening with $E_{B-V}(\alpha, \beta)$ up to $0\overset{\mathrm{m}}{.}24$. Around the supershell LMC 6 a reddening up to $0\overset{\mathrm{m}}{.}22$ occurs. Low reddenings show the supershells LMC 3 and LMC 8 with $E_{B-V}(\alpha, \beta)$ down to $0\overset{\mathrm{m}}{.}09$ and $0\overset{\mathrm{m}}{.}11$, respectively.

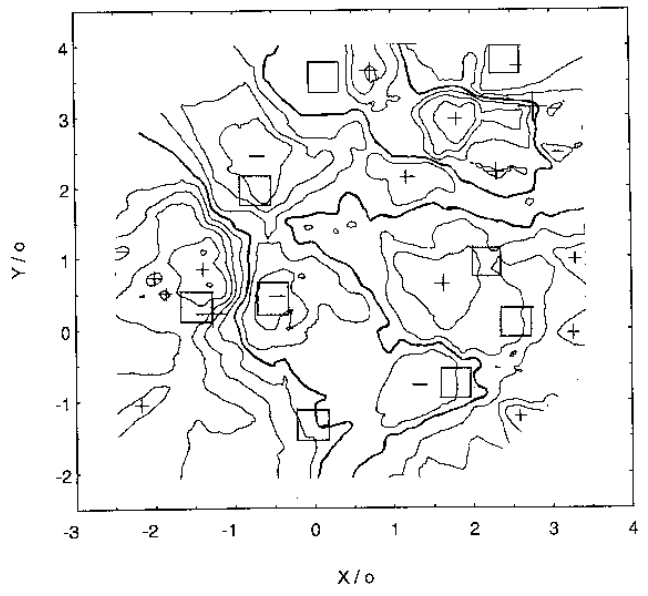

Fig. 17. The reddening distribution in the LMC. The contour lines represent reddenings of $0\overset{\mathrm{m}}{.}10$, $0\overset{\mathrm{m}}{.}15$, $0\overset{\mathrm{m}}{.}20$ and $0\overset{\mathrm{m}}{.}25$, respectively. The contour line for $E_{B-V}(\alpha,\beta) = 0\overset{\mathrm{m}}{.}15$ is stressed. Maxima are marked with "+", minima with "-". The 30 Dor region and the HII region N 11 are marked with crosses. Supershells are marked with larged quadrangles. Cartesian coordinates according to Isserstedt (1975) are used

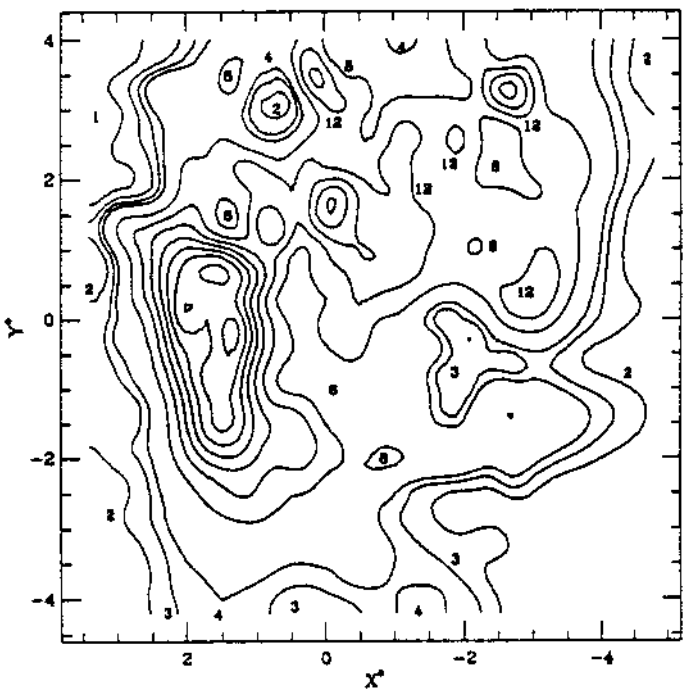

Fig. 18. The total HI column density in the LMC according to Luks & Rohlfs (1992). The contours represent levels of $N_{\mathrm{HI}} = (1, 2, 3, 4, 8, 12, 16, 20, 24, 28, 32)\ 10^{20}\mathrm{cm}^{-2}$. Cartesian coordinates according to Isserstedt (1975) are used

The error of $E_{B-V}(\alpha,\beta)$ is about $0\overset{\mathrm{m}}{.}02$ where many stars per $\square^\circ$ are available, but exceeds $0\overset{\mathrm{m}}{.}05$ where only few stars were observed. Our map shows qualitative good agreement with that of Isserstedt & Kohl (1984). We find, however, higher absolute values as we adopted bluer intrinsic colours as these authors.

5. Comparison with HI and infrared data

Finally we compared our results with maps derived by HI and infrared observations. The agreement of our map with the HI map of Luks & Rohlfs (1992) and the 25 μm and 100 μm IR emission map of Israel & Schwering (1986) is good. The HI map presented in Fig. 18 shows more details, however, as the authors could deal with about 1800 data points while we only had 558. Its resolution, $15'$, is about a factor of two better than that of our map with about $30'$. The IR maps (Figs. 19 and 20) with resolution of $8'$show also more detail. At the edges of our map, especially in the south west and south east, deviations from the HI and IR data occur. They may be caused by the large errors due to the low number of stars available in those regions.

Acknowledgements. We acknowledge gratefully the financial support of this investigation by the Deutsche Forschungsgemeinschaft by grant Schm 160/39-1.

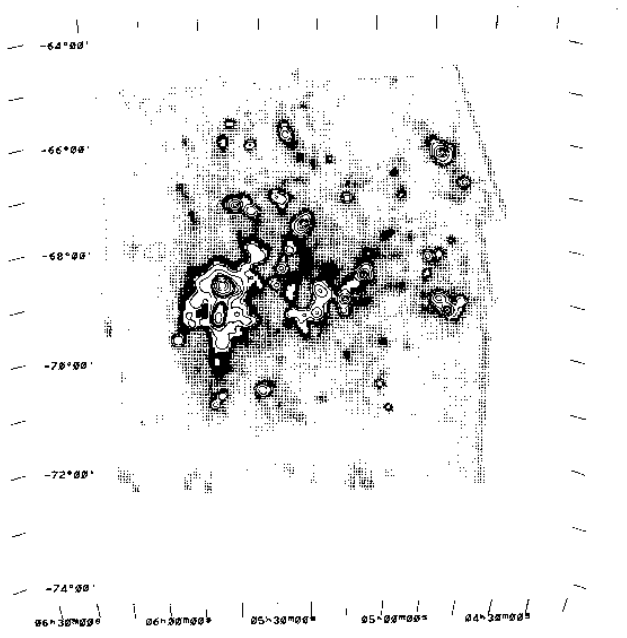

Fig. 19. 25 μm IR emission map of the LMC according to Israel & Schwering (1986)

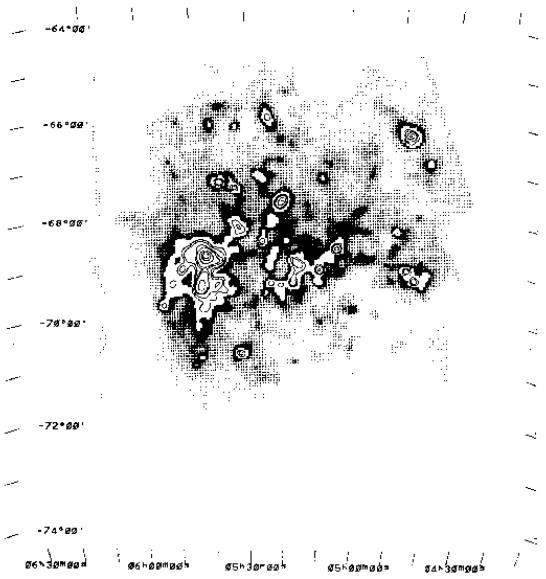

Fig. 20. 100 μm IR emission map of the LMC according to Israel & Schwering (1986)

References

Ardeberg A., Brunet J.P., Maurice E., Prevot L., 1972, A&AS 6, 249

van den Bergh S., 1974, ApJ 193, 63

Brunet J.P., 1975, A&A 43, 345

Cohen R.S., Dame T.M., Garay G., Montani J., Rubio M., Thaddeus P., 1988, ApJ 331, L95

Conti P.S., Garmany C.D., Massey P., 1986, AJ 92, 48

Dachs J., 1972, A&A 18, 271

Feast M.W., Thackeray A.D., Wesselink A.J., 1960, MNRAS 121, 337

Fitzpatrick E.L., 1988, ApJ 335, 703

Gochermann J., Schmidt-Kaler Th., Oestreicher M.O., 1992, A New Data Base of LMC Stars, in: New Aspects of Magellanic Cloud Research, Lec. Not. in Phys. 416, 98

Gochermann J., 1995, PhD thesis, Ruhr-University Bochum (in preparation)

Grieve G.R., Madore B.F., 1986, ApJS 62, 427

Heydari-Malayeri M., Hutsemekers D., 1991, A&A 244, 64

Hobbs L.M., 1974, ApJ 191, 395

Hodge P.W., 1972, PASP 84, 365

Israel F.P., Schwering P.B., 1986, IRAS Observations of the Magellanic Clouds, in: Light on Dark Matter, Astrophysics and Space Science Library Vol. 124. In: Israel F.P. (ed.), p. 383

Isserstedt J., 1975, A&A 41, 175

Isserstedt J., Kohl W., 1984, A&A 139, 115

Knude J., 1979a, A&A 71, 344

Knude J., 1979b, A&AS 38, 407

Luks Th., Rohlfs K., 1992, A&A 263, 41

Massey P., Lang C.C., DeGioia-Eastwood K., Garmany C.D., 1995, ApJ 438, 188

Münch G., 1952, ApJ 116, 575

Oestreicher M.O., Gochermann J., Schmidt-Kaler Th., 1995, A&AS 112, 495

Parker J.W., Garmany C.D., Massey P., Walborn N.R., 1992, AJ 103, 1205

Rousseau J., Martin N., Prevot L., Rebeirot E., Robin A., Brunet J.P., 1978, A&AS 31, 243

Schatzmann E., 1950, Ann. Astrophys. 13, 367

Scheffler H., 1967a, Z. Astrophys. 65, 60

Scheffler H., 1967b, Z. Astrophys. 66, 33

Schmidt-Kaler Th., 1977, A&A 54, 771

Spitzer L., 1978, in Physical Processes in the Interstellar Medium. Wiley, New York, p. 156

Stock J., Osborn W., Ibañez M., 1976, A&AS 24, 35